

This is an electronic reprint of the original article. This reprint may differ from the original in pagination and typographic detail.

Beyond ray optics absorption of light in CsPbBr₃ perovskite nanowire arrays studied experimentally and with wave optics modelling

Anttu, Nicklas; Zhang, Zhaojun; Wallentin, Jesper

Published in:
Nanotechnology

DOI:
[10.1088/1361-6528/ad1160](https://doi.org/10.1088/1361-6528/ad1160)

E-pub ahead of print: 15/12/2023

Document Version
Final published version

Document License
CC BY

[Link to publication](#)

Please cite the original version:

Anttu, N., Zhang, Z., & Wallentin, J. (2023). Beyond ray optics absorption of light in CsPbBr₃ perovskite nanowire arrays studied experimentally and with wave optics modelling. *Nanotechnology*, 35(9), Article 095203. Advance online publication. <https://doi.org/10.1088/1361-6528/ad1160>

General rights

Copyright and moral rights for the publications made accessible in the public portal are retained by the authors and/or other copyright owners and it is a condition of accessing publications that users recognise and abide by the legal requirements associated with these rights.

Take down policy

If you believe that this document breaches copyright please contact us providing details, and we will remove access to the work immediately and investigate your claim.

PAPER • OPEN ACCESS

Beyond ray optics absorption of light in CsPbBr₃ perovskite nanowire arrays studied experimentally and with wave optics modelling

To cite this article: Nicklas Anttu *et al* 2024 *Nanotechnology* **35** 095203

View the [article online](#) for updates and enhancements.

You may also like

- [\(Invited\) Effect of Junction Resistance on the Percolation Conductivity of Metal Nanowire Networks for Transparent Conductors](#)
Shreshtha Mishra, Ying Xue, Nicholas Fata et al.
- [Modeling and Analysis of Electrodeposition in Porous Templates](#)
Alta Fang and Mikko Haataja
- [Modal analysis of resonant and non-resonant optical response in semiconductor nanowire arrays](#)
Vilgail Dagt and Nicklas Anttu

PRIME
PACIFIC RIM MEETING
ON ELECTROCHEMICAL
AND SOLID STATE SCIENCE

HONOLULU, HI
Oct 6–11, 2024

Abstract submission deadline:
April 12, 2024

Learn more and submit!

Joint Meeting of
The Electrochemical Society
•
The Electrochemical Society of Japan
•
Korea Electrochemical Society

Beyond ray optics absorption of light in CsPbBr₃ perovskite nanowire arrays studied experimentally and with wave optics modelling

Nicklas Anttu¹ , Zhaojun Zhang²  and Jesper Wallentin² 

¹Physics, Faculty of Science and Engineering, Åbo Akademi University, FI-20500 Turku, Finland

²Synchrotron Radiation Research and NanoLund, Department of Physics, Lund University, Box 124, Lund 22100, Sweden

E-mail: jesper.wallentin@sljus.lu.se

Received 4 October 2023, revised 10 November 2023

Accepted for publication 30 November 2023

Published 15 December 2023



CrossMark

Abstract

We study experimentally and with wave optics modelling the absorption of light in CsPbBr₃ perovskite nanowire arrays fabricated into periodic pores of an anodized aluminum oxide matrix, for nanowire diameters from 30 to 360 nm. First, we find that all the light that couples into the array can be absorbed by the nanowires at sufficient nanowire length. This behavior is in strong contrast to the expectation from a ray-optics description of light where, for normally incident light, only the rays that hit the cross-section of the nanowires can be absorbed. In that case, the absorption in the sample would be limited to the area fill factor of nanowires in the hexagonal array, which ranges from 13% to 58% for the samples that we study. Second, we find that the absorption saturates already at a nanowire length of 1000–2000 nm, making these perovskite nanowires promising for absorption-based applications such as solar cells and photodetectors. The absorption shows a strong diameter dependence, but for all diameters the transmission is less than 24% already at a nanowire length of 500 nm. For some diameters, the absorption exceeds that of a calculated thin film with 100% coverage. Our analysis indicates that the strong absorption in these nanowires originates from light-trapping induced by the out-of-plane disorder due to random axial position of each nanowire within its pore in the matrix.

Supplementary material for this article is available [online](#)

Keywords: absorption, light-trapping, perovskite nanowire array

1. Introduction

Semiconductors hold a central position as materials for optoelectronics applications [1, 2], since they can be used for absorbing incident photons, for example for solar cells and photodetectors, and for emitting photons, for example for light-emitting diodes (LEDs) and lasers. Silicon (Si) is the

semiconductor that dominates microelectronics industry and solar cell industry. III–V semiconductors, like InP and GaAs, and their ternary compounds like GaInP, on the other hand offer tailored electrical and optical properties [3], but at a premium price compared to Si. Recently, metal halide perovskites (MHPs), such as CsPbBr₃ and CH₃NH₃PbI₃ [4], have appeared as a new class of semiconductors that could combine affordable manufacturing cost with tailorable optical and electrical properties, suitable for example for high-efficiency photovoltaics [5, 6] and LEDs [7].

Semiconductors are commonly developed in planar structures. However, semiconductors in nanowire form have



Original content from this work may be used under the terms of the [Creative Commons Attribution 4.0 licence](#). Any further distribution of this work must maintain attribution to the author(s) and the title of the work, journal citation and DOI.

attracted recent interest for optoelectronic applications [8], offering unique opportunities to tune electric and optical properties. From previous studies on III–V semiconductor and Si nanowire arrays, we know that the optical response of nanowires cannot be properly analyzed with ray optics [9–12]. In a ray-optics description, for light that is incident at normal angle to the array, that is, parallel to the nanowire axis, only the rays that impinge at the top of the nanowires propagate into the nanowires. In this way, the amount of light that can be absorbed by the nanowires is limited by their area coverage. However, since the diameter of nanowires is comparable to the wavelength of light, the wave-optical nature of light manifests itself. When light is described as an electromagnetic wave, the wave has a spatial extent, such that light cannot pass between the nanowires without interacting with the nanowires. Importantly, light that would pass between nanowires in a ray-optics description can actually couple efficiently into the nanowires when the wave-properties of light are taken into account [13]. In this way, even a relatively sparse nanowire array can absorb almost all the above-bandgap incident light [14, 15]. Furthermore, the reflection loss in a nanowire array can be substantially lower than in a corresponding planar sample [14, 15]. Thus, in nanowire form, semiconductors could offer further optimized optical response compared to their thin-film counterpart [11, 12].

MHP nanowires have appeared much more recently than Si and III–V ones [16], and they have found interest for optoelectronic applications [17, 18], such as flexible photovoltaics [19], tandem solar cells [20], photodetectors [21], LEDs [22, 23] and x-ray detectors [24, 25]. In contrast to planar technology, the nanowire-array geometry readily allows for a curved surface, as for example in hemispherical MHP-nanowire photodetectors for a biomimetic eye [26]. CsPbBr₃ perovskite nanowires fabricated into an anodized aluminum oxide (AAO) matrix have shown long-term stability in photoluminescence (PL) [27] and x-ray [24] measurements. Similarly, CsPbI₃ perovskite nanowires in AAO have been integrated into photodetectors, showing enhanced phase stability, which was assigned to encapsulation by the AAO [21], with a further demonstration of broadband absorption performance and integration of 1024 pixels [28]. Perovskite nanowires have been also used as dual-mode image sensor for standard and neuromorphic imaging [29] and for laser-based hydrogen chloride gas sensing [30].

In comparison with traditional semiconductor nanowires, the nanophotonic properties of MHP nanowires have not been studied extensively, even though many of the same intriguing optical phenomena should be expected. For optoelectronic applications with MHP nanowire arrays, dedicated studies of their optical response are needed. Similarly, when using MHP nanowire x-ray scintillators [31], the modified optical response is important to understand due to the outcoupling and re-absorption of x-ray-generated bandgap emission of photons.

Here, we study experimentally and with optics modelling the reflection, transmission, and absorption of incident light in an array of CsPbBr₃ nanowires in an AAO membrane

template for varying nanowire diameter, nanowire length, and array period. We find that the absorption saturates already at a nanowire length of 1000–2000 nm, making these CsPbBr₃ nanowires promising for absorption-based applications such as solar cells and photodetectors. The optical properties depend, in addition to the nanowire length, on the nanowire diameter and array period, which highlights the need for wave optics simulations to understand such structures and devices.

2. Methods

2.1. Samples

The MHP nanowires are fabricated into pores that go through a 50 μm thick AAO membrane. The pores of diameter D are placed in a hexagonal pattern of period P . In the synthesis, also the nanowire length L is controlled by changing the precursor amount or concentration. The nanowire synthesis starts at a random depth in each AAO pore, giving rise to randomness in the nanowire position into the membrane, but with a well-defined length for each nanowire (see figure 1(a) for a schematic and figure 1(b) for a scanning electron microscope (SEM) image). For details of the fabrications, see [31]. To allow optics measurements on the thin and brittle AAO membranes, each membrane is attached to a 0.10 mm thick microscope coverslip (see figure 1(c)).

We study here six different combinations for the diameter and period: (1) $D = 30$ nm and $P = 65$ nm; (2) $D = 60$ nm and $P = 100$ nm; (3) $D = 90$ nm and $P = 125$ nm; (4) $D = 170$ nm and $P = 450$ nm; (5) $D = 250$ nm and $P = 450$ nm; and (6) $D = 360$ nm and $P = 450$ nm. The standard deviation for $D = 30, 60, 90, 170, 250,$ and 360 nm is estimated to 5, 10, 10, 20, 20, and 20 nm, respectively [27]. The standard deviation in pore position from the perfect hexagonal array for $P = 65, 100, 125,$ and 450 nm is estimated to 5, 10, 10, and 20 nm, respectively [27]. For the nanowire length, we consider for each combination of diameter and period five different nominal values: $L = 0, 0.5 \mu\text{m}, 1 \mu\text{m}, 2 \mu\text{m},$ and $10 \mu\text{m}$ (for $L > 0$, deviation from the nominal L is estimated to 20% relative and the standard deviation in L is estimated to 30% relative—see supplementary material figure S1). Thus, we consider in total 30 different samples, with $L = 0$ corresponding to the empty AAO matrices before nanowire synthesis.

2.2. Measurements

We have performed reflection (R), transmission (T) and absorption (A) measurements. We measured at the middle of each sample—the position might slightly vary between $R, T,$ and A measurements since a repositioning of sample and illumination spot is performed between the measurements.

The R and T measurements are performed in an s 2 inch integrating sphere, similarly as in [32]. The A measurements are performed with the sample in the middle of a 6 inch LabSphere integrating sphere. For all measurements, an OceanOptics fiber spectrometer is used for recording the

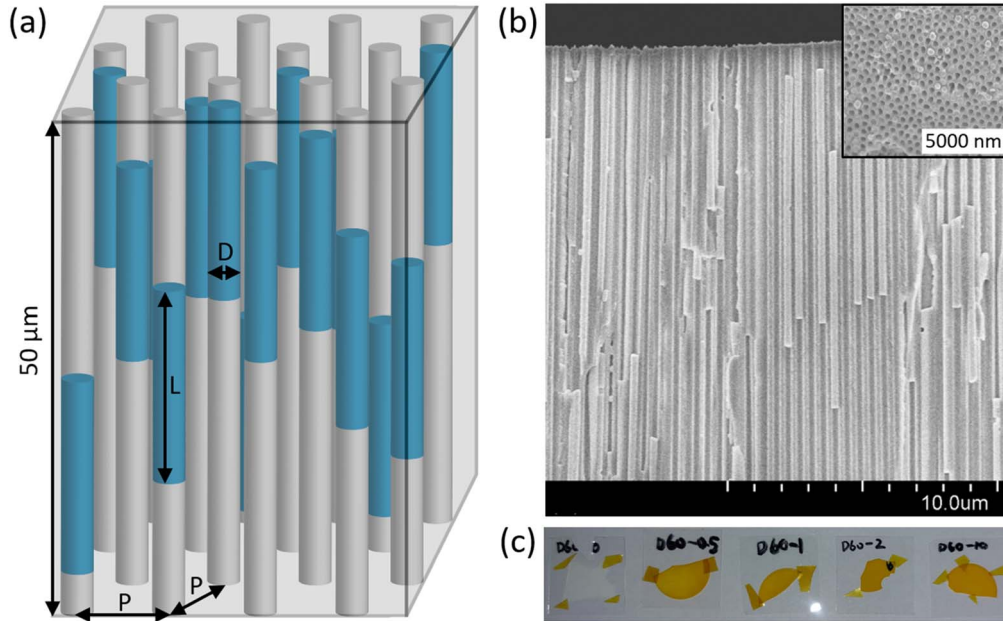


Figure 1. (a) Schematic of the $50\ \mu\text{m}$ thick AAO membrane with a hexagonal array of pores with period P and diameter D . Here, in blue, we indicate a single nanowire of length L at a random depth in each pore. (b) Side-view SEM image, after cleaving, of the top part of the sample with $D = 250\ \text{nm}$, $P = 450\ \text{nm}$, and $L = 10\ \mu\text{m}$. The scalebar is $10.0\ \mu\text{m}$. The inset shows a top-view SEM image of the sample (for top-view SEM images of all the samples, see figure S2 in the supplementary material). (c) Photograph of the samples with $D = 60\ \text{nm}$ and $P = 100\ \text{nm}$. The samples are in order of $L = 0, 0.5, 1, 2$ and $10\ \mu\text{m}$ from left to right. $L = 0$ corresponds to the reference AAO-only sample that has no nanowires. Each sample is attached on an $18 \times 18\ \text{mm}$ microscope glass coverslip with small pieces of yellow tape.

signal. For R and T measurements, a lamp with output coupled to a fiber and collimating lens at the end of the fiber was used for the illumination, giving a spot size of approximately $3\ \text{mm}$ in diameter. For A measurements, light from a light bulb was let through a small opening in a screen and focused onto the sample with a lens, giving a similar spot size of approximately $3\ \text{mm}$ in diameter. In this configuration, the A measurements give considerably noisier spectra than the R and T measurements.

Sample, reference, and background measurements are performed as in [32]. We have ascertained with the direct absorption measurements with the $L = 0$ samples in the middle of an integrating sphere that the absorption in the AAO is negligible (see figure S3 in the supplementary material).

3. Results and discussion

We show in figure 2 the R and T spectra for the $D = 60\ \text{nm}$ and $P = 100\ \text{nm}$ samples, that is, five in total with $L = 0, 0.5, 1, 2,$ and $10\ \mu\text{m}$. The spectra for all the 30 different (D, P, L) samples are shown in the supplementary material (figures S4 and S5, as well as the much noisier A measurements in figure S6).

CsPbBr_3 is a semiconductor with bandgap at approximately $530\ \text{nm}$ in wavelength at room temperature [33]. In our measurements on the nanowire samples, that is, when $L > 0$, starting from the bandgap wavelength, we see with increasing wavelength (i) a rapid increase in transmission (figure 2(a)), (ii) a rapid increase in reflection (figure 2(b)),

and a rapid drop in absorption toward zero-values (figure 2(c)). In general, we will use saturation of T toward a zero-value as a measure of when absorption saturates with increasing L . Alternatively, we could study the convergence of A toward a limiting value, but that limiting value depends on the remaining reflectance of the sample, and that reflectance is not known *a priori*.

For the AAO-only sample, that is, when $L = 0$, in figure 2(a), we find that T shows a rather wavelength-independent value of approximately 80%. For $L = 500\ \text{nm}$, the transmittance for wavelengths below the bandgap wavelength drops to approximately 10%, and already for $L = 1000\ \text{nm}$, we have very close to zero-values for T in that wavelength range. With increasing L , there is a clear red-shift of the edge in the transmittance (and in figure 2(c), we see a similar shift for absorption edge), which will be discussed further below.

For an overview of the optical properties in the absorption region of all the 30 samples considered, we have extracted in figure 3(a) for them the average T for $475 < \lambda < 525\ \text{nm}$, that is, in the region just below the bandgap wavelength [for completeness, we show the corresponding A in figure 3(b)]. We show this dependence as a function of L in figure 3, together with the calculated values for bulk CsPbBr_3 . We find for all samples saturation of transmission toward a zero value at a nanowire length L of just $1000\text{--}2000\ \text{nm}$. Already at lengths of $L = 500\ \text{nm}$ all diameters show less than 24% transmission, with some below the calculated value for bulk CsPbBr_3 . Thus, these MHP nanowires appear very promising for light-absorption applications. To investigate the dependence on D and P on the absorption, due to the saturation with L , only the samples with

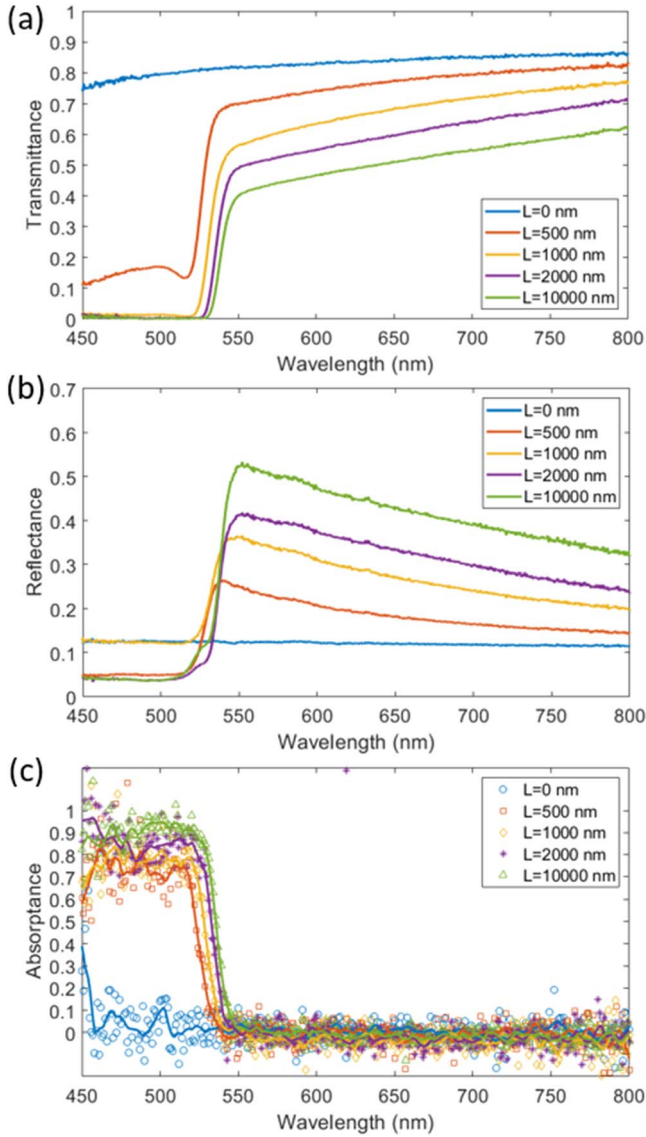


Figure 2. Measured (a) transmittance, (b) reflectance, and (c) absorbance for the samples with $D = 60$ nm and $P = 100$ nm. Note that in the absorbance measurements, the noise level is rather large for wavelengths below 460 nm.

$L = 500$ nm give meaningful differences between the samples (see table S1 in the supplementary information). We do not find a clear dependence on neither D , P nor D/P , which calls for future studies on a larger set of D and P values to elucidate on how these parameters affect the absorption.

Importantly, the saturation of the transmission toward a zero-value shows that all the light that couples into the MHP sample can be absorbed by the nanowires. This behavior is in strong contrast to the expectation from a ray description of light where for normally incident light, only the rays that hit the cross-section of the nanowires can be absorbed. In that case, the absorption in the sample would be limited to the area fill factor of nanowires in the hexagonal array (which ranges from 13% to 58% for these samples).

To better understand the optical response of these MHP nanowires, we show the refractive index of the CsPbBr₃ perovskite [34] in figure 4. We find that $\text{Re}(\underline{n})$, the real part of

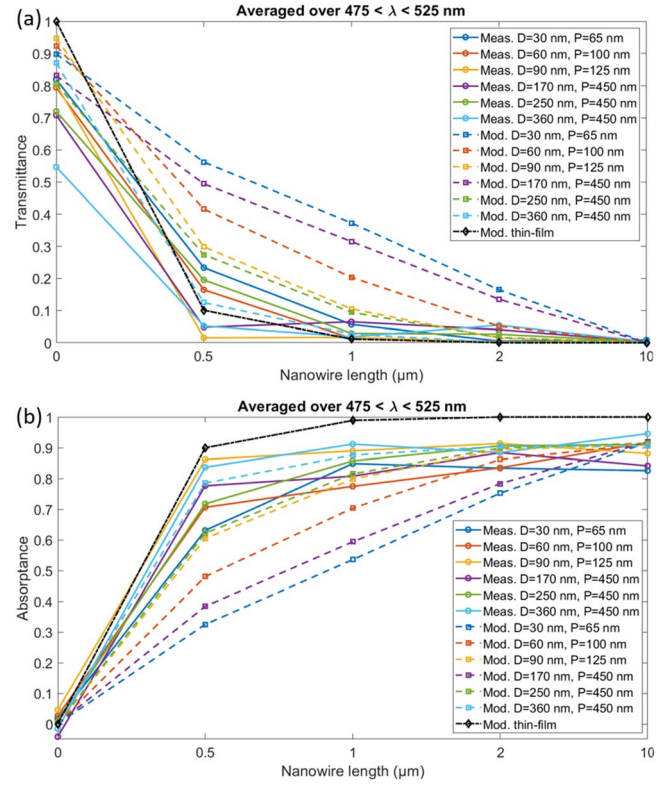


Figure 3. Average (a) transmittance and (b) absorbance for $475 < \lambda < 525$ nm as a function of nanowire length L for the six sets of samples of different D and P . The circle markers with solid lines are from measurements and the square markers with dashed lines are from modelling. In addition, we show in (a) modelled transmittance and in (b) modelled absorbance of a thin-film of the MHP of thickness equal to the stated nanowire length, with perfect anti-reflection coatings on both front and rear interface (diamond markers). The horizontal scale is set non-uniform in order to emphasize the rapid variation at short nanowire lengths. The lines connecting the markers are included to guide the eye.

the refractive index, is in the range of 2.1–1.8 in this 450–800 nm wavelength range that we study. The imaginary part $\text{Im}(\underline{n})$ of the refractive index gives rise to an absorption length $L_{\text{abs}}(\lambda) = (4\pi \text{Im}[n(\lambda)]/\lambda)^{-1}$ on the order of 200 nm for the $475 < \lambda < 525$ nm range in figure 3. Based on this absorption length, which applies for bulk material, it is promising that we find absorption saturation already at a nanowire length of $L = 1000$ nm. For example for the $D = 170$ nm and $P = 450$ nm sample, the area fill factor of nanowires in the hexagonal array is 13%. If we would assume that the absorption length scales with the same factor, we would thus expect an absorption length on the order of 2000 nm. In other words, these nanowires, where absorption saturates for a nanowire length of 1000–2000 nm, absorb considerably stronger than expected from such an assumption (for saturation in absorption, we would expect to need 2–3 absorption lengths of material thickness). Indeed, when we compare the measured transmission in the nanowires with the modelled transmission in the corresponding MHP thin-film of the same thickness as the nanowire length (dashed-dotted line in figure 3(a)), we find a rather similar drop toward a zero-value with increasing nanowire length and film thickness. Here,

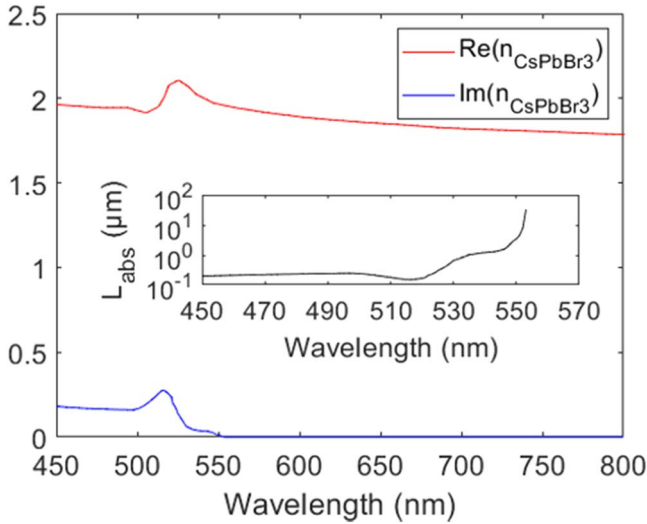


Figure 4. Real and imaginary part of the refractive index, n , for CsPbBr_3 , extracted from [34]. The inset shows the absorption length $L_{\text{abs}} = \left[\frac{4\pi \text{Im}(n)}{\lambda} \right]^{-1}$ for CsPbBr_3 from the extracted values for $\text{Im}(n)$.

perfect anti-reflection coating was assumed at the top and bottom of the thin-film, leading to $A \rightarrow 100\%$ with increasing L for the modelled thin-film in figure 2(c). For further comparison, we show modelled spectra in figure S8 in the supplementary material for the perovskite thin-film, including reflection losses, similarly as in [35, 36] for comparing planar and nanostructured systems. By comparing these spectra for the thin film with the measured spectra in figure 2 for the perovskite nanowire sample with $D = 60$ nm and $P = 100$ nm (and for all the samples in figures S4–S6 in the supplementary material), we indeed see that the perovskite nanowire arrays absorb almost as strongly as the thin-film.

3.1. Modelled optical response

By using the refractive index for the MHP and AAO, we can in principle model the optical response of the samples by solving the Maxwell equations for the scattering of light [37]. However, the modelling of the optical response of our system with out-of-plane disorder in the form of random vertical placement of each nanowire in the $50 \mu\text{m}$ thick AAO matrix is beyond our present computational resources.

To obtain related modelling results to compare with, we have instead modelled the optical response of a simpler system consisting of a perfectly ordered array of nanowires, that is, without in-plane or out-of-plane disorder (see supplementary material for technical details of the optics modelling). Such ordered arrays of MHP nanowires can in principle be fabricated [38], but the range of nanowire diameters and lengths of interest for this study makes an experimental path very demanding and beyond the scope of the present paper—we turn instead to modelled results for comparison.

We note that the modelled $D = 360$ nm and $P = 450$ nm sample and $D = 90$ nm and $P = 125$ nm sample show rather similar D/P ratio of 0.80 versus 0.72 but the $D = 360$ nm and $P = 450$ nm sample shows much faster convergence in

modelling toward $T = 0$ with increasing L (dashed lines in figure 3, which are obtained from the modelled spectra in supplementary material figure S10). This highlights the need for wave-optics simulations for appropriate modelling of the optical response of these MHP nanowires. In other words, effective medium theories relying on just the D/P ratio for describing the optical response of the sample are not sufficient. Typically, weak absorption of normally incident light in small-diameter semiconductor nanowires originates from the electrostatic screening due to contrast in the refractive index between the nanowire and the surrounding, while for larger-diameter nanowires, nanophotonic resonances can set in to enhance the absorption [11, 12].

In the modelling of the perfect array, we tend to find a slower saturation of the absorption with increasing nanowire length than in the measurements (dashed lines versus solid lines in figure 3). That is, the experimental nanowire arrays with random vertical position for each nanowire shows substantially stronger absorption than the modelled perfect arrays. Only the $D = 360$ nm and $P = 450$ nm sample shows similar absorption in measurements and modelling while all the other samples show noticeably stronger absorption in measurements. Especially surprising, compared to modelled results, is that the $D = 30$ nm and $P = 65$ nm sample also saturates in absorption measurements in the vicinity of a 1000 nm nanowire length; in the modelling, absorption-saturation seems to require a nanowire length toward 10000 nm length. This difference between measurements and modelling indicates that additional light-trapping occurs in the measured samples to boost the absorption compared to in the modelling of the perfectly ordered array.

3.2. Indication of light-trapping

Light-trapping by scattering of light inside a sample to boost absorption is a broad research topic [39, 40]. For such light-trapping, some sort of structuring beyond the fully planar thin-film system is needed. Previous studies have typically considered either (i) grating assisted light-trapping [39], where periodically ordered scatterers such as grating lines or dots/pores scatter light into well-defined directions inside the sample or (ii) in-plane randomness in nanostructure position [41] to scatter light into a broad distribution of angles inside the sample. In both types of light-trapping, the scattering of light into large angles inside the structure causes a much larger path-length for the light inside the sample to enhance absorption, especially since light propagating at sufficiently large angle inside the sample is prevented, due to total internal reflection, from escaping the sample. In our case, we believe that the strongest light-trapping effect is induced by the out-of-plane (axial) randomness in the nanowire positions within the $50 \mu\text{m}$ thick AAO matrix.

For completeness: we do find some signs of both grating-assisted light-trapping and light-trapping induced by in-plane randomness, that is, due to minor variation in the pore diameter and deviation of pore position from the perfect hexagonal array. Such effects are seen clearly in the AAO-only samples, that is, $L = 0$, for the largest $P = 450$ nm and

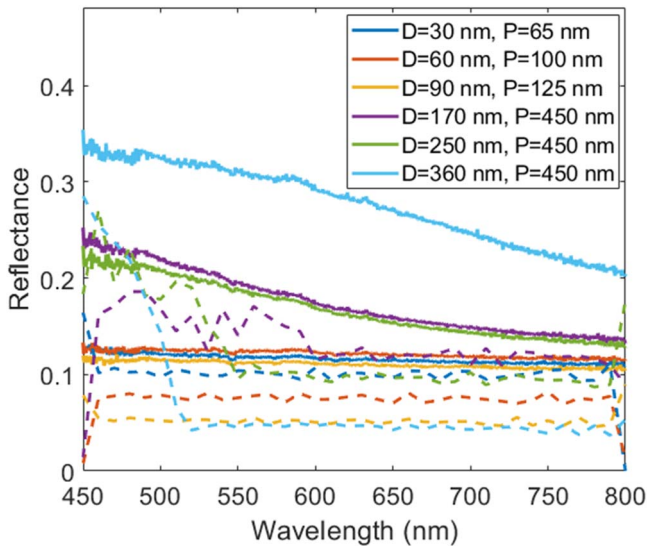


Figure 5. Measured (solid lines) and modelled (dashed lines) reflectance of the AAO samples without MHP nanowires, that is, these samples are with $L = 0$.

$D = 360$ nm. Modelling of the AAO-only array with $P = 450$ nm and $D = 360$ nm, without any disorder or variation in the size or position between the pores, shows a reflectance that starts at 25% at the shortest wavelength considered, but drops to low values of $\approx 4\%$ at $\lambda \approx 520$ nm, and stays at that level up to the longest $\lambda = 800$ nm considered (figure 5). The high reflectance at $\lambda < 520$ nm, and the sudden drop to much lower values at a distinct wavelength, indicates grating-assisted light-trapping [39]. Also the measured reflectance starts at a high value, of approximately 30%, at $\lambda = 450$ nm. However, in strong contrast to the modelled reflectance of the perfectly ordered array, the measured reflectance stays at a high value throughout the measurement range, dropping toward 20% at $\lambda = 800$ nm (figure 5). Thus, for $\lambda > 520$ nm, the measurements yield a much higher reflectance than the modelling. This discrepancy indicates light-trapping into the fabricated membrane for $\lambda > 520$ nm due to the variation in pore size and position that is not included in the modelling—light-trapping in the absence of absorption, as in the AAO-only samples, is known to lead to increased reflectance [32].

For the three smallest- P samples, we see in measurements a flat R at a low level of around 10% for $L = 0$ (figure 5), in good agreement with the values found from modelling of the perfectly ordered AAO-only samples (figure 5). This agreement indicates that in-plane randomness is not enough for light-trapping for those AAO-only samples. However, we did find above a much stronger measured absorption in the corresponding MHP nanowire samples, as compared to modelling of the perfectly ordered nanowire array. This stronger absorption in measurements indicates that out-of-plane light-trapping induced by nanowires at varying depth contributes to absorption strongly. Importantly, also these samples with the smallest P considered show with increasing L a peak of up to $R \approx 50\%$ at $\lambda = 550$ nm, that is, just beyond the bandgap wavelength, and this R decreases

toward long wavelengths (figure 2(b)). Such a strong peak in R is one sign for light-trapping in nanowire arrays [32].

Finally, we see a possible sign of light-trapping through the red-shift of the absorption edge with increasing nanowire length in figure 2, as well as in Figures S3-S5 in the supplementary material. Importantly, in these measurements, the slope in these curves appear to stay constant around the bandgap but red-shift with increasing length, with a shift of approximately 10 nm when L increases from 500 to 10 000 nm. In strong contrast, in the modelled absorption curves (figure s11 in the supplementary material), the cut-off wavelength for absorption occurs at a well-defined wavelength (around 558 nm) and the slope in the absorption curve becomes steeper and steeper with increasing L . For completeness—we need to state that we have no reason to believe that the underlying refractive index of the MHPs would change with increasing L in such a way which would cause a red-shifting absorption edge. Instead, we assign the red-shift in the measurements to light-trapping effects beyond those present in the modelling of the perfect array.

3.3. Comparison to absorption and light-trapping in nanowire arrays of other semiconductor materials

We have previously studied III–V semiconductor nanowire arrays, such as InP and GaAs nanowires. In such cases, the refractive index of the semiconductor is in the vicinity of 3.5, thus much higher than the ≈ 2 of the currently studied CsPbBr₃ (see figure 4). Importantly, the III–V semiconductors then give a large refractive index contrast to the surrounding, up to 3.5/1 when surrounded by air, in which case the optical response becomes strongly diameter-dependent [11, 42]. Then, dielectric screening is a strong effect at small diameter to suppresses absorption, while nanophotonic resonances boost absorption at a suitably chosen, larger, diameter [11]. Simultaneously, fine-tuning of in-plane light-trapping in ordered III–V nanowire arrays is possible [43].

In contrast, we find a much smaller contrast for the current CsPbBr₃ nanowires embedded in the AAO, with approximately a refractive index of 1.75 for the AAO [44]. Therefore, we do not expect as strong dielectric screening, nanophotonic resonances, or in-plane light-trapping in the present case. Free-standing MHP nanowires can be grown using various techniques [16, 38, 45], which increases the contrast from the current 2.0/1.75 to 2.0/1.0. However, a study of free-standing nanowires with varying diameter, period, and length is beyond the scope of the present study. Nevertheless, our results highlight the need for wave optics modelling of MHP nanowires to understand their optical properties.

The effect of disorder compared to a perfectly ordered array has been studied in vertical Si nanowire arrays [46, 47] and InP nanowire arrays [48, 49]. However, in those cases, the focus has been on lateral disorder in aperiodic arrays that are still placed in a single plane. In contrast, we study here a case with pre-dominantly out-of-plane disorder.

4. Conclusions

We studied the absorption of light in CsPbBr₃ perovskite nanowires that show out-of-plane disorder with random axial position of each nanowire within each pore of an AAO matrix. We find much stronger absorption in the measurements of the disordered array compared to optics modelling of a perfectly periodic array with all the nanowires in the same plane. Therefore, the strong absorption in the measurements is assigned to light-trapping induced by the out-of-plane disorder. To further elucidate the effect of out-of-plane disorder, we highlight the need for future experimental studies on MHP nanowires, all placed in the same plane, as well as numerically very demanding modelling studies of MHP nanowire arrays with out-of-plane disorder.

Acknowledgments

NA acknowledges financial support from the Waldemar von Frenckell Foundation. This research was funded by the European Research Council (ERC) under the European Union's Horizon 2020 research and innovation program (Grant Agreement 801847). This research was also funded by the Olle Engkvist Foundation, NanoLund, and the Swedish Research Council Vetenskapsrådet grant 2021-04273.




Data availability statement

All data that support the findings of this study are included within the article (and any supplementary files).

Conflict of interests

The authors declare no competing interests.

ORCID iDs

Nicklas Anttu  <https://orcid.org/0000-0002-7626-5107>
 Zhaojun Zhang  <https://orcid.org/0000-0003-0678-1699>
 Jesper Wallentin  <https://orcid.org/0000-0001-5909-0483>

References

- [1] Saleh B E A and Teich M C 2007 *Fundamentals of Photonics* 2nd edn (Wiley)
- [2] Sze S M, Li Y and Ng K K 2021 *Physics of Semiconductor Devices* (Wiley)
- [3] Vurgaftman I, Meyer J R and Ram-Mohan L R 2001 Band parameters for III–V compound semiconductors and their alloys *J. Appl. Phys.* **89** 5815–75
- [4] Green M A, Ho-Baillie A and Snaith H J 2014 The emergence of perovskite solar cells *Nat. Photon.* **8** 506–14
- [5] Green M A, Dunlop E D, Yoshita M, Kopidakis N, Bothe K, Siefert G and Hao X 2023 Solar cell efficiency tables (version 62) *Prog. Photovolt. Res. Appl.* **31** 651–63
- [6] Chin X Y *et al* 2023 Interface passivation for 31.25%-efficient perovskite/silicon tandem solar cells *Science* **381** 59–63
- [7] Liu X-K, Xu W, Bai S, Jin Y, Wang J, Friend R H and Gao F 2021 Metal halide perovskites for light-emitting diodes *Nat. Mater.* **20** 10–21
- [8] Zhang Y, Wu J, Aagesen M and Liu H 2015 III–V nanowires and nanowire optoelectronic devices *J. Phys. D: Appl. Phys.* **48** 463001
- [9] Hu L and Chen G 2007 Analysis of optical absorption in silicon nanowire arrays for photovoltaic applications *Nano Lett.* **7** 3249–52
- [10] Lin C and Povinelli M L 2009 Optical absorption enhancement in silicon nanowire arrays with a large lattice constant for photovoltaic applications *Opt. Express* **17** 19371–81
- [11] Anttu N 2013 Geometrical optics, electrostatics, and nanophotonic resonances in absorbing nanowire arrays *Opt. Lett.* **38** 730–2
- [12] Anttu N 2023 Absorption of light in vertical III–V semiconductor nanowires for solar cell and photodetector applications *Crystals* **13** 1292
- [13] Wallentin J *et al* 2013 InP nanowire array solar cells achieving 13.8% efficiency by exceeding the ray optics limit *Science* **339** 1057–60
- [14] Anttu N, Abrand A, Asoli D, Heurlin M, Åberg I, Samuelson L and Borgström M 2014 Absorption of light in InP nanowire arrays *Nano Res.* **7** 816–23
- [15] Hu S, Chi C-Y, Fountaine K T, Yao M, Atwater H A, Dapkus P D, Lewis N S and Zhou C 2013 Optical, electrical, and solar energy-conversion properties of gallium arsenide nanowire -array photoanodes *Energy Environ. Sci.* **6** 1879–90
- [16] Zhang D, Eaton S W, Yu Y, Dou L and Yang P 2015 Solution-phase synthesis of cesium lead halide perovskite nanowires *J. Am. Chem. Soc.* **137** 9230–3
- [17] Zhang D, Zhang Q, Zhu Y, Poddar S, Zhang Y, Gu L, Zeng H and Fan Z 2023 Metal Halide perovskite nanowires: synthesis, integration, properties, and applications in optoelectronics *Adv. Energy Mater.* **13** 2201735
- [18] Kumar G S, Sumukam R R, Rajaboina R K, Savu R N, Srinivas M and Banavoth M 2022 Perovskite nanowires for next-generation optoelectronic devices: lab to fab *ACS Appl. Energy Mater.* **5** 1342–77
- [19] Zhu Y *et al* 2022 Three-dimensional nanopillar arrays-based efficient and flexible perovskite solar cells with enhanced stability *Nano Lett.* **22** 9586–95
- [20] Raja W, Schmid M, Toma A, Wang H, Alabastri A and Proietti Zaccaria R 2017 Perovskite nanopillar array based tandem solar cell *ACS Photon.* **4** 2025–35
- [21] Waleed A, Tavakoli M M, Gu L, Hussain S, Zhang D, Poddar S, Wang Z, Zhang R and Fan Z 2017 All inorganic cesium lead iodide perovskite nanowires with stabilized cubic phase at room temperature and nanowire array-based photodetectors *Nano Lett.* **17** 4951–7
- [22] Zhang Q, Zhang D, Gu L, Tsui K-H, Poddar S, Fu Y, Shu L and Fan Z 2020 Three-dimensional perovskite nanophotonic wire array-based light-emitting diodes with significantly improved efficiency and stability *ACS Nano* **14** 1577–85
- [23] Zhang Q *et al* 2019 Efficient metal halide perovskite light-emitting diodes with significantly improved light extraction on nanophotonic substrates *Nat. Commun.* **10** 727
- [24] Dierks H, Zhang Z, Lamers N and Wallentin J 2023 3D x-ray microscopy with a CsPbBr₃ nanowire scintillator *Nano Res.* **16** 1084–9
- [25] Wibowo A, Sheikh M A K, Diguna L J, Ananda M B, Marsudi M A, Arramel A, Zeng S, Wong L J and

- Birowosuto M D 2023 Development and challenges in perovskite scintillators for high-resolution imaging and timing applications *Commun. Mater.* **4** 21
- [26] Gu L et al 2020 A biomimetic eye with a hemispherical perovskite nanowire array retina *Nature* **581** 278–82
- [27] Zhang Z, Suchan K, Li J, Hetherington C, Kiligaridis A, Unger E, Scheblykin I G and Wallentin J 2021 Vertically aligned CsPbBr₃ nanowire arrays with template-induced crystal phase transition and stability *J. Phys. Chem.C* **125** 4860–8
- [28] Gu L et al 2016 3D arrays of 1024 pixel image sensors based on lead halide perovskite nanowires *Adv. Mater.* **28** 9713–21
- [29] Long Z, Ding Y, Qiu X, Zhou Y, Kumar S and Fan Z 2023 A dual-mode image sensor using an all-inorganic perovskite nanowire array for standard and neuromorphic imaging *J. Semicond.* **44** 092604
- [30] Markina D I, Anoshkin S S, Masharin M A, Khubezhov S A, Tzibizov I, Dolgintsev D, Terterov I N, Makarov S V and Pushkarev A P 2023 Perovskite nanowire laser for hydrogen chloride gas sensing *ACS Nano* **17** 1570–82
- [31] Zhang Z, Dierks H, Lamers N, Sun C, Nováková K, Hetherington C, Scheblykin I G and Wallentin J 2022 Single-crystalline perovskite nanowire arrays for stable x-ray scintillators with micrometer spatial resolution *ACS Appl. Nano Mater.* **5** 881–9
- [32] Anttu N, Dągtyć V, Zeng X, Otnes G and Borgström M 2017 Absorption and transmission of light in III–V nanowire arrays for tandem solar cell applications *Nanotechnology* **28** 205203
- [33] Mannino G, Deretzis I, Smecca E, La Magna A, Alberti A, Ceratti D and Cahen D 2020 Temperature-dependent optical band gap in CsPbBr₃, MAPbBr₃, and FAPbBr₃ single crystals *J. Phys. Chem. Lett.* **11** 2490–6
- [34] Yan W et al 2020 Determination of complex optical constants and photovoltaic device design of all-inorganic CsPbBr₃ perovskite thin films *Opt. Express* **28** 15706–17
- [35] Cong S et al 2019 Fabrication of nickel oxide nanopillar arrays on flexible electrodes for highly efficient perovskite solar cells *Nano Lett.* **19** 3676–83
- [36] Zhao J, Sun P, Wu Z, Li J, Wang X, Xiao T, Yang L, Zheng Z and Huang Z 2021 Titanium nanopillar arrays functioning as electron transporting layers for efficient, anti-aging perovskite solar cells *Small* **17** 2004778
- [37] Anttu N, Mäntynen H, Sorokina A, Turunen J, Sadi T and Lipsanen H 2021 Applied electromagnetic optics simulations for nanophotonics *J. Appl. Phys.* **129** 131102
- [38] Zhang Z, Lamers N, Sun C, Hetherington C, Scheblykin I G and Wallentin J 2022 Free-standing metal halide perovskite nanowire arrays with blue-green heterostructures *Nano Lett.* **22** 2941–7
- [39] Yu Z, Raman A and Fan S 2010 Fundamental limit of nanophotonic light trapping in solar cells *PNAS* **107** 17491–2946
- [40] Mokkaapati S and Catchpole K R 2012 Nanophotonic light trapping in solar cells *J. Appl. Phys.* **112** 101101
- [41] Battaglia C et al 2012 Light trapping in solar cells: can periodic beat random? *ACS Nano* **6** 2790–7
- [42] Anttu N and Xu H Q 2013 Efficient light management in vertical nanowire arrays for photovoltaics *Opt. Express* **21** A558–75
- [43] Dągtyć V and Anttu N 2019 Modal analysis of resonant and non-resonant optical response in semiconductor nanowire arrays *Nanotechnology* **30** 025710
- [44] Gervais F 1998 Aluminum oxide (Al₂O₃) *Handbook of Optical Constants of Solids* ed E D Palik (Academic) pp 761–75
- [45] Oksenberg E, Sanders E, Popovitz-Biro R, Houben L and Joselevich E 2018 Surface-guided CsPbBr₃ perovskite nanowires on flat and faceted sapphire with size-dependent photoluminescence and fast photoconductive response *Nano Lett.* **18** 424–33
- [46] Lin C and Povinelli M L 2011 Optimal design of aperiodic, vertical silicon nanowire structures for photovoltaics *Opt. Express* **19** A1148–54
- [47] Sturmberg B C P, Dossou K B, Botten L C, Asatryan A A, Poulton C G, McPhedran R C and de Sterke C M 2013 Absorption enhancing proximity effects in aperiodic nanowire arrays *Opt. Express* **21** A964–9
- [48] Wu D, Tang X, Wang K, He Z and Li X 2017 An efficient and effective design of InP nanowires for maximal solar energy harvesting *Nanoscale Res. Lett.* **12** 604
- [49] Fountaine K T, Cheng W-H, Bukowsky C R and Atwater H A 2016 Near-unity unselective absorption in sparse InP nanowire arrays *ACS Photon.* **3** 1826–32